SAND2022-7902C

Proceedings of the ASME 2022
Internal Combustion Engine Division Fall Technical Conference
ICEF2022
October 16-19, 2022, Indianapolis, Indiana

ICEF2022-95118

DRAFT: INVESTIGATION ON THE EFFECTS OF PASSIVE PRE-CHAMBER IGNITION SYSTEM AND GEOMETRY ON ENGINE KNOCK INTENSITY

Francesco Di Sabatino
CRF, Sandia National Laboratories
Livermore, CA

Pablo Martinez-Hernandiz
CMT, Universitat Politècnica de València,
Valencia, Spain

Ricardo Novella Rosa
CMT, Universitat Politècnica de València,
Valencia, Spain

Isaac Ekoto
CRF, Sandia National Laboratories
Livermore, CA

ABSTRACT

The effects of passive pre-chamber (PC) geometry and nozzle pattern as well as the use of either conventional spark or non-equilibrium plasma PC ignition system on knocking events were studied in an optically-accessible single-cylinder gasoline research engine. The equivalence ratio of the charge in the main chamber (MC) was maintained equal to 0.94 at a constant engine speed of 1300 rpm, and at constant engine load of 3.5 bar indicated mean effective pressure for all operating conditions. MC pressure profiles were collected and analyzed to infer the amplitude and the frequency of pressure oscillations that resulted in knocking events. The combustion process in the MC was investigated utilizing high-speed excited methylidyne radical (CH) chemiluminescence images. The collected results highlighted that PC volume and nozzle pattern substantially affected the knock intensity (KI), while the use of the non-equilibrium plasma ignition system exhibited lower KI compared to PC equipped with a conventional inductive ignition system. It was also identified that knocking events were likely not generated by conventional end gas auto-ignition, but by jet-related phenomena, as well as jet-flame wall quenching. The relation between these phenomena and PC geometry, nozzle pattern, as well as ignition system has been also highlighted and discussed.*

Keywords: Turbulent jet ignition; Pressure oscillations; Non-equilibrium plasma discharges; End gas auto-ignition; Jet absolute instabilities; Jet-flame wall quenching

NOMENCLATURE

AHRR	Apparent heat release rate [J/°]
ATDC	After TDC
c	Speed of sound [m/s]
CA	Crank angle
CH*	Excited methylidyne radical
d	Nozzle diameter [m]
f	Frequency [Hz]
IDT	Ignition delay time [s]
IMEPg	Gross indicated mean effective pressure [bar]
ISP	Inductive ignition system
KI	Knock intensity [bar^2]
MAPO	Max. amplitude of pressure oscillations [bar]
MC	Main chamber
m_e	Mass entrained by the jet [kg]
NRP	Nanosecond repetitively pulsed
P	Pressure at knock onset [bar]
PC	Pre-chamber
P_{filt}	Filtered pressure data [bar]
PSD	Power spectral density [bar^2/Hz]
RHR	Remaining heat release [%]
rpm	Rotations per minute
SCRE	Single-cylinder research engine
SER	Single energy ratio []
SI	Spark-ignition
ST	Spark timing [CA]
St	Strouhal number [-]
T	Temperature at knock onset [K]
t	Time for the jets to reach the MC wall [s]
TDC	Top dead center
U_0	Initial velocity of the jets [m/s]
x	Bore radius [m]
β	Constant for the simplified wave equation [-]
ΔCAs	Range of crank angle succeeding [CA]
ΔCAp	Range of crank angle preceding [CA]
ρ_0	Initial density of the jet core [kg/m^3]
ρ_1	Initial density of the gas in the MC [kg/m^3]

Φ Equivalence ratio

1. INTRODUCTION

Lean combustion is a promising technology to reduce spark-ignition (SI) engine emissions and improve performance [1]–[3]. However, poor ignition stability has been highlighted as a drawback of this combustion mode [4]. Several techniques have been considered to improve the repeatability of ignition processes to include igniters that use non-equilibrium plasma discharges [5]–[7] as well as pre-chambers (PC) [8]–[10].

Pre-chamber ignition is characterized by generated jets of combustion products or active radicals that propagate from the pre-chamber into the main chamber and serve as a distributed source of ignition. Passive PCs – without auxiliary fueling into the pre-chamber – have demonstrated effectiveness to enhance combustion stability [11], [12].

Several studies have been performed to assess the effects of PC on knock propensity in SI engines. Knocking events can appear in PC-equipped engines when an equivalence ratio close to stoichiometry is used for the main charge [13]–[15]. Attard et al. [13] investigated the extension of the knock limit of a 0.6 liter single cylinder research engine by passive PCs as well as by PCs with auxiliary fuel injection. They observed a significant extension of the knock limit using PCs and they related this extension to the very fast burn rates generated by the multiple, widely distributed ignition sites produced by the PC, which rapidly consumed the main charge preventing strong end gas auto-ignition events. Similarly, Cui et al. [14] analyzed the effect of PC volume on the knocking characteristics of a SI aircraft piston engine. They highlighted that PCs with larger volume can better suppress knocking events. As presented in [13], the authors attributed the suppression to faster main chamber (MC) flame development due to multiple ignition sites generated by the PC that in turn led to rapid burning of the end gases by flames before end gas auto-ignition could occur. Liu et al. [15] investigated the effects of PC on knocking characteristics of a 0.5 liter SI single cylinder engine. They observed that the engine equipped with a PC knocked more severely than without, if the spark timing was not adjusted. However, they highlighted that, at constant knock intensity (KI), the introduction of PC resulted in fewer knocking events compared to conventionally ignited engines.

Even though the cited studies provided useful information on the effects of PCs on knocking phenomena in SI engines, no detailed analyses were performed to assess if end gas auto-ignition was the main source of the pressure fluctuations. Moreover, all the experiments were performed in metal engines, so no images of the combustion process in the MC were collected to support the conclusions presented in [13]–[15]. Additionally, only conventional inductive ignition systems were implemented in these studies.

As previously mentioned, end gas auto-ignition has been considered as the only possible source of pressure fluctuations that could trigger knocking events in PC-ignited engines. However, the presence of high-temperature turbulent jets propagating in a lower-temperature environment could serve as source of pressure fluctuations, as described in [16], [17]. Biswas et al. [17] analyzed the ejection and propagation of a single high-temperature turbulent jet in a quiescent lower-temperature constant volume vessel. They observed the presence of strong pressure oscillations and thermoacoustic instabilities generated by the unstable shear layer between the hot turbulent jet and the quiescent cold environment as well as by the feedback loop between the acoustic field of the vessel and the corrugated surface area of the jet. The results presented in [16], [17] highlighted that pressure oscillations can be directly generated by PC jets, however these studies were performed in a constant volume vessel. Therefore, it is of interest to investigate if jet-related phenomena could be responsible for the generation of pressure oscillations and knocking events in an engine that features much more dynamic fluid motion compared to a constant volume vessel.

The objectives of this study are a) to investigate the effects of PC geometry and ignition system on knocking events, b) to verify if end gas auto-ignition is the phenomenon controlling the knock intensity and c) to identify possible jet-related phenomena that can also drive knocking events.

2. EXPERIMENTAL SETUP AND PROCEDURE

2.1 Experimental setup

The Sandia 4-stroke, optically accessible single-cylinder research engine (SCRE) developed by General Motors (SG2) was used to perform the experimental campaign; a schematic is provided in Figure 1.

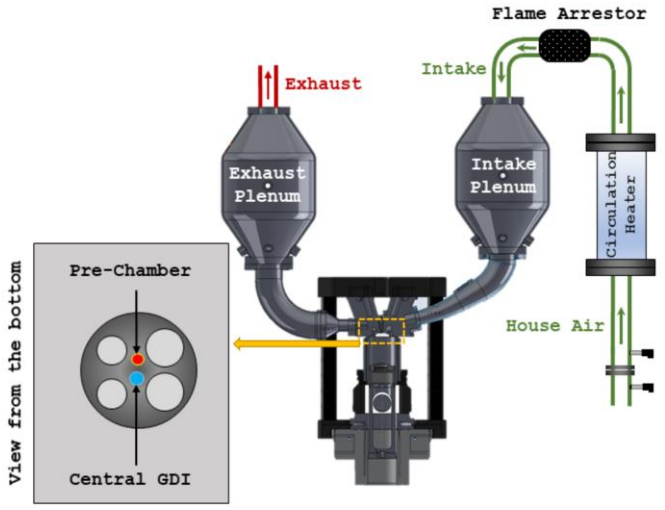

FIGURE 1: SCHEMATIC OF THE SCRE.

Detailed characteristics of this engine were discussed in a previous study [18], with only a brief discussion given here. The engine featured a 13:1 geometric compression ratio when a conventional spark plug was used, although the effective compression ratio is much lower due to large crevice regions. The presence of PC reduced the compression ratio to 12.5 and 12.6 for PC 1 and PCs 2 and 3, respectively. A single fuel

injection at 330 crank angles (CA) before top dead center compression (TDC) was used to generate a homogeneous fuel-air charge in the main chamber. The engine speed was kept constant at 1300 revolutions per minute (rpm) using a motoring dynamometer connected to a BEI Precision optical encoder with 0.1 CA resolution to measure crank location. A research gasoline with an 87 anti-knock index (RD5-87) was used as the fuel. A piezo-electric pressure transducer (Kistler 6135A) installed in the engine head was used to measure in-cylinder pressure. Time-resolved (40 kHz) image sets of excited methylidyne radical (CH*) chemiluminescence from main chamber combustion were visualized through a piston bowl mounted window using a Photron SA-Z high-speed camera connected to a Lambert high-speed HiCATT intensifier. The camera was equipped with 105 mm UV f/2.8 Nikkor lens and a 5 nm narrowband filter centered at 420 nm to isolate CH* emission. These images were collected to investigate the jet-controlled combustion process and flame propagation in the main chamber [19]. A schematic of the imaging setup is provided in Figure 2.

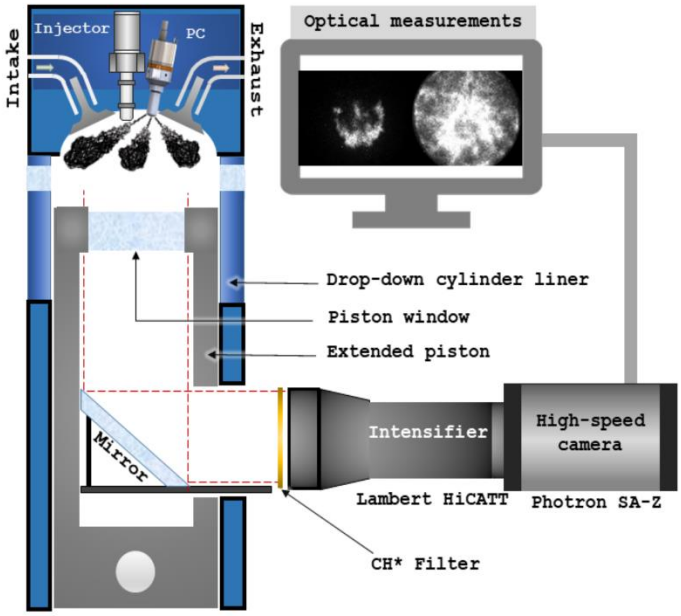

Figure 2 SCEMATIC OF THE CH* CHEMILUMINESCENCE IMAGING SETUP.

The pre-chamber featured a custom 2-piece design with a main body that housed the igniter and an embedded AVL GH14P fast response pressure-transducer, while the interchangeable tip contained the PC volume and nozzle pattern. The PC volume had a funnel that fed into an elongated 3 mm wide throat just prior to the exit nozzles. Three tips were explored following design guidance from CMT-Motores Térmicos, with main features summarized in Table 1 and a schematic shown in Figure 3.

A conventional inductive spark plug ignition system (ISP) with a fixed 4 ms charge time was utilized as the baseline pre-chamber igniter. The second ignition system generated NRP plasma discharges utilizing a nanosecond DC pulse generator (Transient Plasma Systems Inc. SSPG-101-HF). Pulse number and primary voltage were adjusted to the minimum respective values to maintain a stable engine combustion.

Table 1: MAIN GEOMETRICAL PARAMETERS OF THE PRE-CHAMBERS.

Tip	PC 1	PC 2	PC 3
Volume [cm3]	2.0	1.7	1.7
Radial nozzle number	6	6	6
Radial nozzles diameter [mm]	0.8	0.8	1.2
Axial nozzle number	1	1	0
Axial nozzle diameter [mm]	1.0	1.0	-
Total nozzle area [mm^2]	3.8	3.8	6.8
Nozzles tangential angle [º]	12.5	12.5	12.5
Radial nozzle cone angle [º]	150	150	150

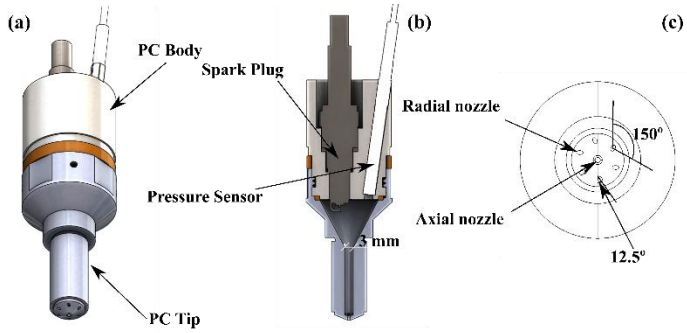

Figure 3 SCHEMATIC OF THE PC ASSEMBLY. THE PC 1 AND 2 FEATURE RADIAL AND AXIAL NOZZLES, WHILE PC 3 HAS ONLY RADIAL NOZZLES. NOZZLE PATTERN, TANGENTIAL, AND CONE ANGLES ARE HIGHLIGTED IN THE BOTTOM VIEW OF THE PC, SHOWED IN PART C.

2.2 Experimental procedure and methodology

Steps for data collection and processing were as follows. The engine was motored for at least 1000 cycles with the intake air flow adjusted to the desired value to warm up the pre- and main chamber surfaces. The engine was then fired while adjusting the spark timing (ST) to obtain a stable combustion process in the main chamber with the lowest fueling rate possible and a constant gross indicated mean effective pressure (IMEPg) of 3.5 bar. In-cylinder pressure was recorded for 100 cycles once combustion performance and exhaust pollutant emissions were stable. At the same time, 200 CH* chemiluminescence images were collected at a rate of 40 kHz (0.2 CA resolution at 1300 rpm) in 10 of the 100 cycles, starting one CA before ST. Once data collection was complete, the engine was stopped with main chamber surfaces cleaned and the rings oiled. A constant equivalence ratio (ϕ) equal to 0.94 was used for all operating conditions discussed here. The fixed experimental procedures, load, and rpm were expected to reproduce consistent engine thermal conditions when PC geometry and ignition system were changed.

Apparent heat release rate (AHRR) and heat losses for the main chamber were evaluated based on a two-zone combustion model with a modified Woschni correlation, optimized for lean gasoline compression combustion [20], including energy and

mass exchange between PC and MC. The total cumulative heat released was also evaluated with the same model.

The KI is defined here as the integral of the power spectral density (PSD) in the frequency domain. It was evaluated by applying a bandpass filter (5 to 30 kHz) to single-cycle pressure traces, with the PSD of the filtered signals calculated in MATLAB. The PSD average and standard deviation were evaluated for each operating condition with KI calculated as follows:

$$KI\ [bar^2] = \int_{5\ kHz}^{30\ kHz} PSD(f)\ df \quad (1)$$

Where *f* is the frequency. The integral of PSD has been selected as a measure of knock intensity since it defines the energy content of the pressure signal at the specific excited acoustic modes of the MC, and therefore, it is less sensitive to background noise, compared to the maximum amplitude of pressure oscillations (MAPO) [21].

The CA of knock onset was defined based on the single energy ratio (SER) described in [22] as shown in Eq. 2.

$$\mathrm{SER} = \frac{\left(\int_{\Delta CAs} {P_{filt}}^2 dCA\right)^2}{\left(\int_{\Delta CAp} {P_{filt}}^2 dCA\right)^{0.5}} \quad (2)$$

Where P_{filt} is the single-cycle filtered main chamber pressure trace. ΔCAs and ΔCAp are the range of CA succeeding and preceding the specific CA. The range of CA selected to evaluate the CA onset was taken from -100 to 100° that covered all possible heat release during the cycle. The CA of knock onset corresponded to the CA at which SER was maximum. Both the average and standard deviation of CA of knock onset were evaluated for all the experimental conditions.

3. NUMERICAL SETUP AND PROCEDURE

The radial acoustic modes of the main chamber were numerically evaluated based on a simplified wave equation presented in [23], and reported in Eq. 3.

$$\mathrm{f}\,(Hz) = c\sqrt{\frac{\beta^2}{4\pi^2}} \quad (3)$$

Where c is the speed of sound of the gases in the main chamber evaluated based on the results of the two-zone combustion model introduced in the previous section, and β is a scaling factor that depends on a constant and on the bore radius of the engine. These evaluated frequencies were compared to experimentally obtained values to identify the acoustic modes of the MC excited during knocking events.

To assess if conventional end gas auto-ignition was possible at the conditions investigated, two sets of Ansys Chemkin-Pro [24] homogeneous reactor simulations were performed to estimate possible ignition delay times (IDT). For both sets, a PACE-20 chemical kinetic surrogate mechanism was used to represent the RD5-87 gasoline [25]. For the first set of homogeneous reactor simulations, pressure was fixed to the 100-cycle ensemble averaged pressure profile for each condition. Five additional individual cycle pressure profiles were also run to ensure a representative spread of conditions. Temperature and pressure were initialized with conditions at 55 CA before TDC (see cyan circle in Fig. 4), with the initial temperature provided from the output of the two-zone combustion model described in Section 2.2.

The second set of homogeneous reactor simulations was at constant pressure, fixed either to the value at TDC compression (see magenta square in Fig. 4) or at the maximum of the cycle (see green circles in Fig. 4). As for the first set, five additional individual cycle pressure profiles were implemented to ensure a representative spread of conditions. Additional simulations were performed with the initial temperature artificially increased by 100 K to simulate the presence of hot spots. For both sets of simulations, the IDT was defined based on a temperature threshold of 1500 K.

The PC radial jet momentum, spreading, and thermodynamic characteristics were evaluated using GT-POWER-based numerical models informed by measured PC and MC pressure profiles. These jet properties were used to estimate the time-resolved mixing and thermodynamic state of the jet, which in turn was used to evaluate potential sources of jet-induced knock. For these models, the pre- and main chamber were connected by a series of hole and pipe templates that replicated the PC nozzles. The PC was modeled as a non-moving piston to obtain the pressure evolution as well as mass and energy exchange between both chambers. Heat release was modeled as a Wiebe function that best patched the experimental data. Mass flow rate and gas-exit velocity from the PCs were modeled for a single radial PC nozzle. Calculated jet momentum flux was used as an input for a 1D jet model introduced in the next paragraph. Gases in both chambers were modeled as homogeneous mixtures of combustion products (CO, CO_2, H_2O and N_2) and unburnt gases (air and fuel mixture).

The 1D jet model was developed from a modified diesel spray model to allow the simulation of the gas jet ejection process from the pre-chamber nozzles. A series of assumptions were formulated to calculate the jet penetration length that included consideration of turbulent mixing of hot PC jets with MC mixtures and free-jet propagation with no interaction with piston surfaces [26].

4. RESULTS AND DISCUSSION

In this section the collected results are presented. First, 100-cycle ensemble averaged MC pressure and apparent heat release rate profiles are described. Second, filtered pressure data, PSD as a function of frequency, and the CA of knock onset are discussed. Third, KI is presented with trends compared to parameters related to end gas auto-ignition to verify if this phenomenon could be responsible for observed knock. Finally, possible other phenomena that could be responsible for knocking events are presented and discussed.

4.1 Main chamber pressure and AHRR profiles

Ensemble averaged MC pressure and AHRR profiles are reported in Figure 4. Since these profiles were previously presented and examined in [27], [28], only a brief description is provided here with relevant features discussed. While MC pressure profiles were similar across all PC geometries and ignition systems up to the ejection of the jets from the PC into the MC (around TDC compression), the differences in pressure profiles between 0 and 30 CA generated AHRR profiles that had substantial variations. Specifically, PC 1 and PC 2 featured similar profiles when the ISP ignition systems was utilized. Conversely, with the NRP igniter, PC 1 had an advanced initial raise and higher peak value as well as a narrower profile as compared to PC 2. For PC 3, the AHRR profile had a lower peak value and a broader profile for both ignition systems due to the absence of the axial nozzle that led to strong centralized ignition for PC 1 and PC 2. All AHRR profiles featured bi-modal heat release impulses that were attributed to sequential ignition of cylinder core mixtures followed by subsequent ignition in the squish region [27].

4.2 Power spectral density and CA of knock onset

While ensemble averaged pressure traces provide important information on general MC combustion trends, single-cycle pressure profiles are required to analyze knocking events. An example single-cycle pressure trace for PC 1 with the ISP igniter and corresponding filtered pressure data (P_{filt}) are plotted in Figure 5. Similar profiles were obtained for the other PC-igniter configurations. Pressure oscillations were observed with amplitudes between 0.4 to 0.6 bar. From Figure 6, up to 3 narrowband peaks were observed in the PSD profiles for each igniter. A comparison between numerically and experimentally evaluated frequencies for each peak is reported in Table 2. The change in ignition system or PC geometry had no effect on peak frequency.

If compared with the frequency of the acoustic modes evaluated using Eq. 3, the three peaks corresponded to the first, second, and third radial acoustic mode of the MC. The 1st mode exhibited numerical and experimental frequencies that were in good agreement, while a substantial difference was observed for the 2nd and 3rd mode. This difference could be related to the presence of mean flow, turbulence, and variable characteristics of the gas in the MC during the engine cycle that were not considered in Eq. 3. Additional analysis is needed to further investigate these effects. It is important to highlight that the 2nd and 3rd radial modes were observed only for PC 1. A possible explanation could be related to the bigger volume of PC 1 (see Table 1) that could serve as an acoustic cavity with impact on the MC acoustic field that could excite other acoustic modes. Since the definition of engine "knock" is somewhat subjective, the presence of non-zero amplitude pressure oscillations synchronized with the radial acoustic modes of the MC and the presence of the distinct audible "knock" sound during experiments, defined the existence of knocking events in this work.

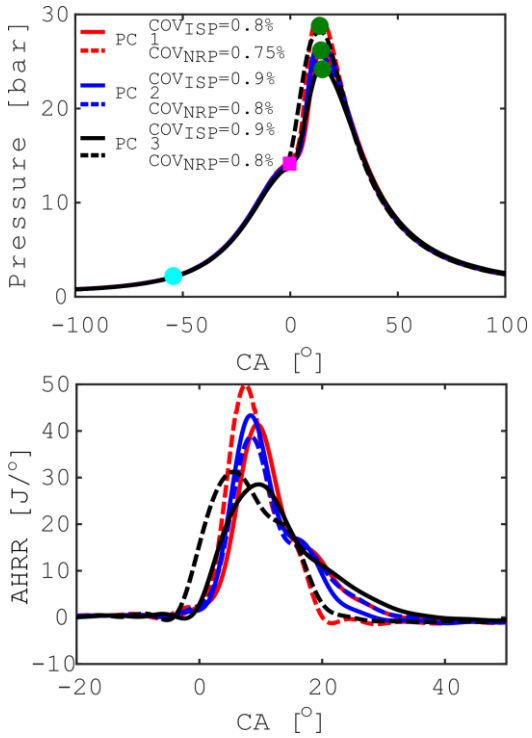

FIGURE 4: 100-CYCLE ENSEMBLED AVERAGE OF THE MC PRESSURE (TOP) AND AHRR (BOTTOM) PROFILES. THE ISP (SOLID LINE) AND THE NRP (DASHED LINE) IGNITION SYSTEMS ARE HIGHLIGHTED. THE COV OF $IMEP_g$ IS PRESENTED IN THE LEGEND.

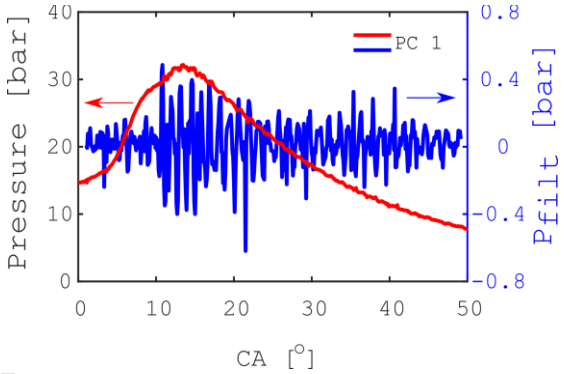

FIGURE 5: EXAMPLE OF SINGLE-CYCLE MC PRESSURE PROFILES (RED) AND P_{FILT} (BLUE) FOR PC 1 WITH ISP IGNITON SYSTEM.

Additional data needed to analyze the knocking events are the CA of knock onset, evaluated from the filtered pressure profiles using Eq. 2 and plotted in Figure 7. All PCs featured similar values of knock onset that were between 6 and 10 CA after TDC compression. The NRP ignition systems substantially retarded knock onset for PC 2, while the standard deviation for PC 1 and PC 3 was too large to properly conclude on the knock onset trend with a change of ignition system.

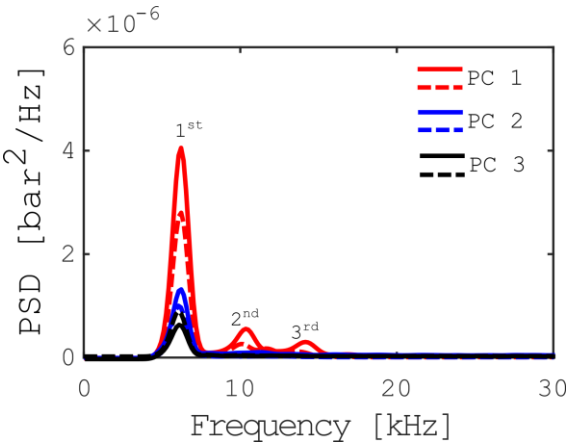

FIGURE 6: AVERAGE PSD AS A FUNCTION OF FREQUENCY FOR ALL PC GEOMETRIES AND IGNITON SYSTEMS, ISP (SOLID LINE) AND NRP (DASHED LINE). THE CORREPSONDING MC RADIAL ACOUSTIC MODE IS HIGHLIGHTED IN THE FIGURE.

Table 2: NUMERICAL AND EXPERIMENTALLY EVALUATED FREQUENCIES OF THE MC ACOUSTIC MODES EXCITED DURING THE KNOCKING EVENTS.

Peak	Numerical frequency (Hz)	Experimental frequency (Hz)
1st	6052	6058
2nd	9925	10600
3rd	12677	14390

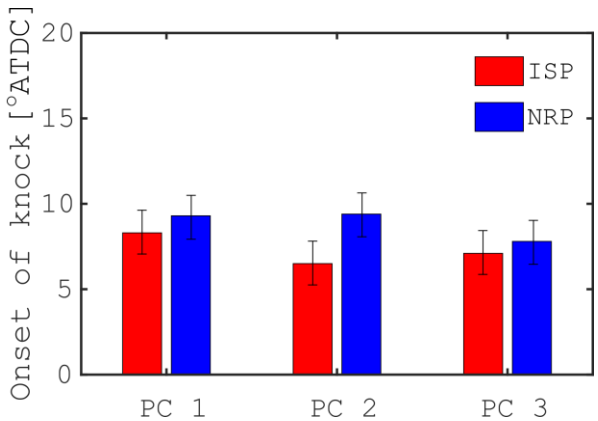

FIGURE 7: AVERAGE CA OF KNOCK ONSET ATDC FOR ALL THE EXPERIMENTAL CONDITIONS ANALYZED IN THIS WORK. ERROR BARS REPRESENT THE STANDARD DEVIATION OF THE DATA.

4.3 Knock intensity and end gas auto-ignition

Values of KI computed from Eq. 1 are plotted in Figure 8 for all the conditions analyzed in this work. PC 1 featured the highest KI, followed by PC 2 and PC 3. Use of the NRP ignition systems reduced KI, with the largest reductions observed for PC 1 and PC 2, with minimal effect on PC 3.

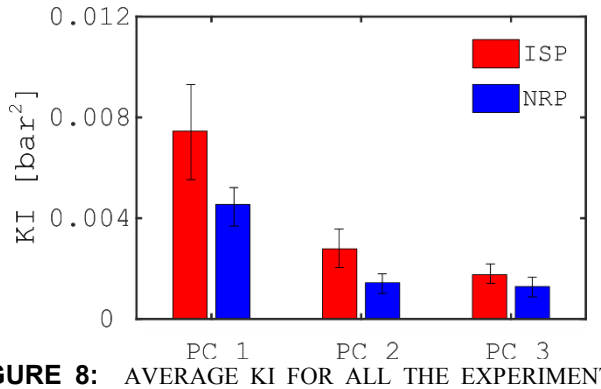

FIGURE 8: AVERAGE KI FOR ALL THE EXPERIMENTAL CONDITIONS ANALYZED IN THIS WORK. ERROR BARS REPRESENT THE STANDARD DEVIATION OF THE DATA.

Since end gas auto-ignition is often responsible for knock, parameters related to this phenomenon were investigated to analyze the trend of KI with changing PC geometry and ignition system. The first parameter investigated was the percentage of remaining cumulative heat release (RHR) at the CA of knock onset, defined here as the ratio of the cumulative heat release at the CA of knock onset to total heat release, which is plotted in Figure 9. A higher percentage of remaining cumulative heat release should result in a higher KI if end gas auto-ignition was responsible for the knock. However, from Figure 9 this was not the case in this work as PC 2 and PC 3 featured a higher percentage of RHR, while having a lower value of KI as compared to PC 1. It also appeared that the use of the NRP igniter slightly reduced the percentage of RHR for all PC geometries, although as stated previously, these trends are largely within the standard deviation of the measurements.

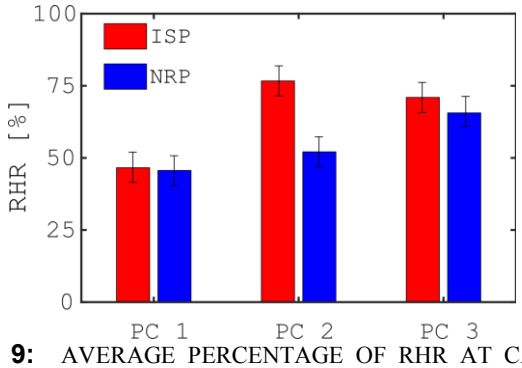

FIGURE 9: AVERAGE PERCENTAGE OF RHR AT CA OF KNOCK ONSET FOR ALL THE EXPERIMENTAL CONDITIONS ANALYZED IN THIS WORK. ERROR BARS REPRESENT THE STANDARD DEVIATION OF THE DATA.

Additional parameters analyzed to verify if end gas auto-ignition was responsible for knocking events were the pressure and temperature at the CA of knock onset, as plotted in Figure 10. No correlation was observed between these parameters and the KI, which suggests that end gas auto-ignition was not responsible for knocking events observed in this work.

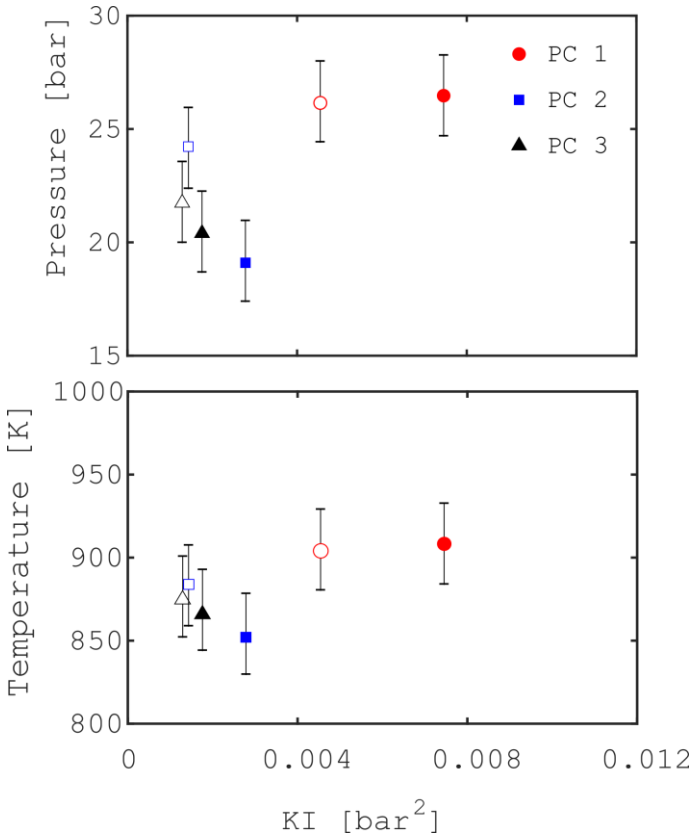

FIGURE 10: AVERAGE PRESSURE (P) AND TEMEPARTURE (T) AT CA OF KNOCK ONSET AS A FUNCTION OF KI. ERROR BARS REPRESENT THE STANDARD DEVIATION OF THE DATA.

To verify these observations further, IDT was numerically evaluated following the procedure presented in Section 3, with values converted to CA. A comparison between the CA of knock onset and the range of CA at which end gas auto-ignition was possible according to chemical kinetics simulations is reported in Figure 11 for the first (top) and the second (bottom) set of simulations. Section 2.2 described the numerical setup for the two sets of simulations. Plain blue and red rectangles highlight knock onset, where the center is the average value, while the height of the rectangle is the standard deviation of the measurements. Blue and red bars with the diagonal black line represent the range of CA at which end gas auto-ignition was possible, according to chemical kinetic simulations. The first set of simulations demonstrate that no end gas auto-ignition was possible for PC 2 and 3, while PC 1 had a 15 – 18 CA retard of auto-ignition compared to the onset of knock. Similarly, the second set of simulations feature substantially retarded end gas auto-ignition events compared to the CA of knock onset. No clear trend was highlighted when the NRP ignition system was utilized instead of the ISP system. From the data presented and analyzed in this section, conventional end gas auto-ignition did not appear to be responsible for the knocking events analyzed in this work.

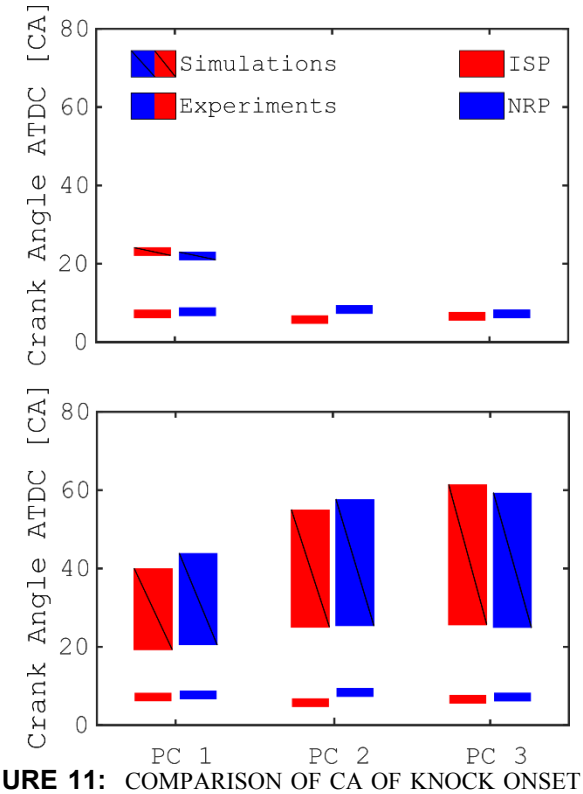

FIGURE 11: COMPARISON OF CA OF KNOCK ONSET AND RANGE OF CA AT WHICH END GAS AUTO-IGNITION WAS POSSIBLE ACCORDING TO NUMERICAL SIMULATIONS IN CA AFTER TDC. THE RESULTS OF THE FIRST (TOP) AND SECOND (BOTTOM) SET OF SIMULATIONS ARE PRESENTED.

4.4 Jet-related phenomena and knocking events

Before analyzing other phenomena that could be responsible for knocking events, a discussion on high-temperature jets exit dynamics is required. Relevant processes have been previously discussed in [27], so only the main features are discussed here. CH* chemiluminescence images of the combustion process in the MC equipped with PC 1 (first row) and 3 (second row) featuring the ISP ignition system are reported in Fig. 12 at different CA during a single cycle. PC 2 had a similar combustion process to PC 1 so it is not shown here. Moreover, only the ISP ignition system is considered, since the NRP featured a similar combustion process.

As shown in Figure 12 (top row), the MC combustion process for PC 1 and 2 was controlled by the ignition and flame propagation generated by the radial and axial jets. The axial jet first ignited the charge in the MC, followed by localized ignition from the radial jets, highlighted by point A and B as well as blue circles. PC 3 did not feature an axial nozzle, so only radial jets controlled the combustion process in the MC. Specifically, an ignition area close to the squish region and an inward-propagating flame were generated by each jet (see Fig. 12, bottom row). It follows from the previous description that PC jets were driving the combustion process in the MC, so it is of interest to analyze if these jets could also be responsible for the generation of heat release fluctuations, and consequently, of pressure fluctuations and knocking events.

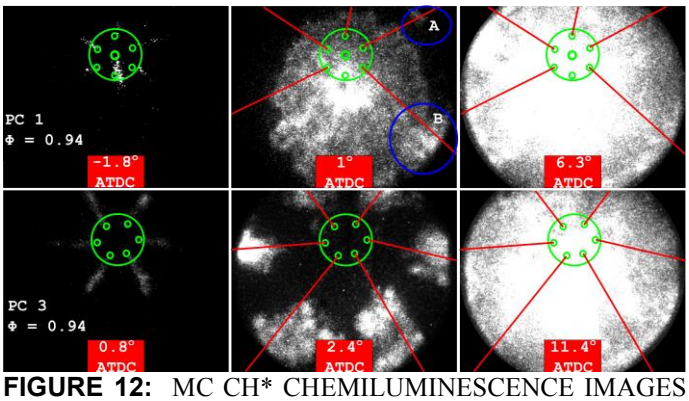

FIGURE 12: MC CH* CHEMILUMINESCENCE IMAGES FOR PC 1 (TOP ROW) AND PC 3 (BOTTOM ROW) EQUIPPED WITH THE ISP IGNITER. GREEN CIRCLES HIGHLIGHT PC TIP AND NOZZLE POSITION, WHILE RED LINES DEFINE RADIAL JETS TRAJECTORY. FIRST IMAGE INTENSITY IN EACH ROW WAS INCREASED TO ENHANCE JET LUMINOSITY.

It has been shown in [17], [29] that turbulent jets propagating in a medium can develop absolute instabilities in the potential core region if the density ratio between the jets and the medium is below 0.72 and the Strouhal number based on the nozzle diameter (d) and initial jet velocity (*Uj*), $St = f\,d/\,Uj$, is below 0.5, where f is the frequency of the excited acoustic modes. These instabilities could result in heat release fluctuations along the shear layer generated by the jets, and consequently, pressure fluctuations could emerge. Even though the theory of absolute instability was developed for steady, constant-composition jets, it could still give valuable information on the conditions analyzed here, where jets were unsteady and with variable composition.

In this work, the density ratio ranged from 0.3 to 0.36 depending on the PC geometry and ignition system. Values were evaluated as the ratio of the density of the burnt gases at the jet core to the density of the unburned charge in the MC when the jets first ejected from the PC nozzle. Density values were extracted from the results of the two-zone combustion model described in Section 2.2. The Strouhal number can also be evaluated based on the initial jet velocity evaluated by the GT-POWER model described in Section 3, the nozzle diameters presented in Table 1, and the frequencies highlighted in Table 2. In this work, the value of St ranged from 0.05 to 0.4 depending on the operating conditions. Therefore, the axial and radial jets considered in this work were absolutely unstable and they could be a source of heat release and pressure oscillations. It is important to stress that this analysis did not consider inherently unstable phenomena, such as turbulence, that could affect the shear layer between the jets and the MC charge, enhancing or diminishing the generation of heat release fluctuations. Further analyses should be carried out to quantify these effects.

An additional jet-related phenomenon that could generate heat release, and consequently, pressure fluctuations, could be the impinging of the jets on the MC walls, followed by the quenching of the flame transported along the jet surface area. As previously mentioned, heat release fluctuations could generate pressure fluctuations, that could trigger knocking events. Pre-mixed flames could produce heat release fluctuations through flame surface area variations, thus flame quenching events would result in a substantial change in flame surface area, and consequently, in strong heat release and pressure fluctuations [30].

Due to the early fuel injection, the MC and PC charge was considered well-mixed before ignition. Moreover, the jets appeared to carry the flame generated inside the PC, since no flame quenching was observed across the PC nozzles (see Fig. 12). Thus, jet-flame quenching at the MC walls could be present in the engine analyzed in this work. The CA at which the radial jets would impinge on the MC wall was evaluated from the GT-POWER simulations and is reported in Fig. 13. No data on the axial jet could be evaluated with the GT-POWER simulations. Comparing Figs. 7 and 13, it appears that the CA at which the radial jets impinged on the MC walls was close to the CA of knock onset; 2-6 CAs separated the two. The NRP ignition systems generated faster radial jets that impinged earlier on the MC walls, however, the CAs of knock onset were slightly more retarded compared to ISP ignition. It is important to highlight this discrepancy but it is also important to note that the SD for the CA of knock onset was large so it is not possible to conclude properly on this trend. Due to the close proximity between the jets impinging the MC walls and the onset of knock, it is interesting to investigate the relation between the jet-flame quenching on the MC walls and the knocking events. As previously mentioned, variation in flame surface area could generate pressure fluctuations, thus it is expected that a jet-flame with a larger cross-section area impinging on the MC walls would generate larger pressure fluctuations, when quenched.

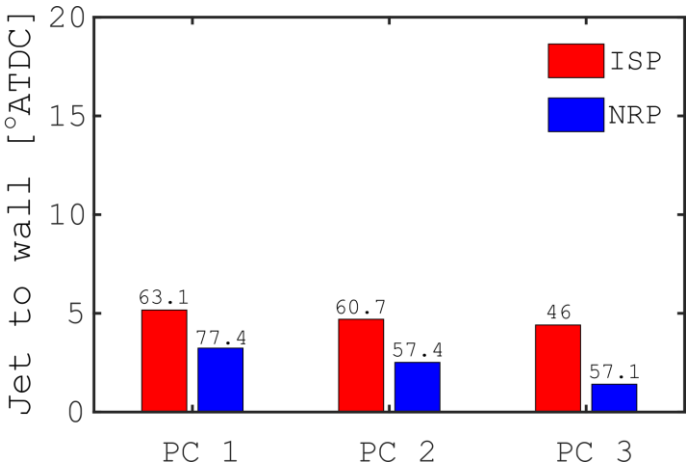

FIGURE 13: CA ATDC AT WHICH THE RADIAL PC JETS COULD IMPINGE ON THE MC WALLS. THE INITIAL JET VELOCITY IS ALSO REPORTED ON TOP OF EACH BAR. CA AND INITIAL VELOCITY WERE EVALUATED THROUGH GT-POWER SIMULATIONS, AS PRESENTED IN [28].

Since it was not possible to directly measure the cross-section area of the jets, an analysis based on the jet entrainment was performed. The total volume of a turbulent jet is

proportional to the mass of gases entrained from the surrounding, thus it is fair to assume that the cross-section area of the jet is also proportional to the mass of gases entrained, if the length of the jet is constant. An estimate of the mass entrained by a turbulent jet is provide by Eq. (4), derived from [31].

$$m_e[kg] = 0.25\, d\, U_0\, x\, (\rho_0 \rho_1)^{1/2} t \qquad (4)$$

m_e is the mass entrained by a radial jet until it reaches the MC wall, d is the diameter of the radial nozzles of the PCs, U_0 is the initial velocity of the radial jets and its value is reported in Fig. 13. Moreover, x is the MC bore radius, t is the time the jets needed to reach the MC walls after ejection from the PCs and it was evaluated from GT-POWER simulations; ρ_0 and ρ_1 are the density of the jet core region and MC charge at the time of ejection, respectively. These densities can be evaluated from the two-zone combustion model presented in Section 2.2, under the assumption that burned gases composed the jets exiting the PC nozzles. Note that Eq. 4 was defined for stationary turbulent jets with no combustion reactions across the shear layer between the jet and the surrounding, while the jets analyzed in this work were unsteady with combustion reactions taking place across the shear layer. However, useful data was obtained that enabled a preliminary relation between KI and m_e/cross-section of the jet-flame to be established. The KI as a function of the normalized value of m_e is reported in Fig. 14 for conditions related to PC 1 and 2. The mass entrained was normalized by the maximum value considering all PC geometries and ignition systems, that was obtained for PC 1 with the ISP ignition system. Fig. 14 shows that there was a good linear relationship (R^2 = 0.93) between the KI and the normalized m_e for PC 1 and 2, highlighting that a higher mass entrained by the jets, i.e. a larger cross-section area of the jet-flame impinging the MC walls, corresponded to a higher KI (higher amplitude of heat release and pressure fluctuations). This linear relation failed for PC 3, so it is not reported in Fig. 14. Possible reasons for the discrepancy could be related to the different nozzle pattern and larger nozzle diameter (see Table. 1), and additional analyses should be carried out in future studies.

The results presented in Fig. 14 highlight a possible reason why the NRP ignition system exhibited a lower KI for all PC geometries. While higher initial jet velocity for the NRP system (see Fig. 13) would result in higher instantaneous mass ejection from the PC nozzle, it also shortened time t. As a result, the overall value of m_e obtained for the NRP ignition system was smaller compared to the ISP, which resulted in a corresponding smaller jet-flame cross-sectional area that was quenched at the MC walls, and consequently, in a lower KI. It is important to highlight that the time it took for the jet-flame to quench should be compatible with the delay between jet impingement on the walls and the start of knocking events. A very simple analysis was carried out to roughly estimate if the delay was sufficiently long using the assumption that the quenching event was instantaneous. Comparing Figures 7 and 13, a delay of 2 to 6 CA was observed between jets imping on the wall and the knock onset, which corresponded to 2 to 5 pressure oscillation periods for the first radial acoustic mode (f = 6058 Hz). The 2 to 5 pressure oscillation periods were probably sufficient to lead to a knock event. However, the presence of multiple jets and quenching events would probably also affect this delay. Therefore, additional analyses are needed to fully quantify the quenching time. Nonetheless, results presented in this section highlight that jet-flame wall quenching events could generate pressure fluctuations that lead to knock, and thus is an important phenomenon to consider for PC-equipped engines.

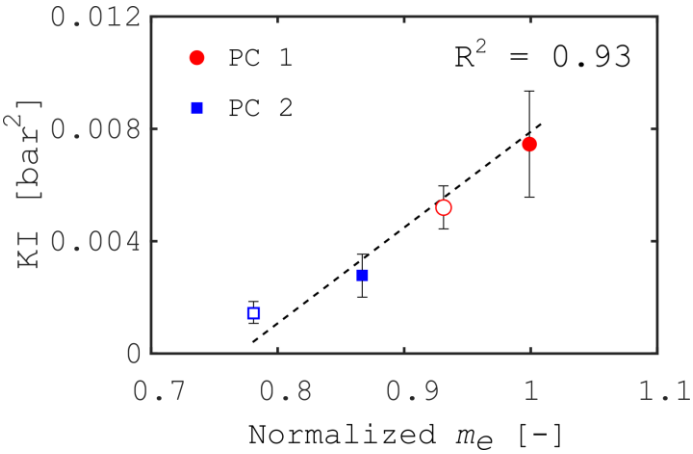

FIGURE 14: KI INTENSITY AS A FUNCTION OF NORMALIZED m_e. THE ERROR BARS CORRESPOND TO THE SD OF THE DATA. THE SOLID AND THE EMPTY SYMBOLS CORRESPOND TO THE ISP AND NRP IGNITON SYSTEMS, RESPECTEVELY.

Note that other jet-related phenomena could contribute to the generation of pressure oscillations, such as jet-to-jet interactions, but the investigation performed in this work did not provide sufficient data to properly analyze these phenomena, thus they are not presented here.

5. CONCLUSION

The manuscript presents an experimental investigation on knocking events generated in a PC-ignited gasoline direct injection engine. Three PC geometries and two PC ignition systems were evaluated. Pressure measurements in the MC were complemented by CH* chemiluminescence images, with these data used to evaluate KI. A simplified wave equation was solved to evaluate the acoustics modes of the MC that were excited during the knocking events. Engine results were complemented by chemical kinetic and GT-POWER simulations. The main findings of this work are reported in the following.

- PSD data showed a narrow band peak center at 6058 Hz that corresponded to the 1st radial acoustic mode of the MC. PC 1 presented two additional narrow band peaks centered at 10600 Hz and 14390 Hz that corresponded to the 2nd and 3rd radial acoustic modes of the MC. The larger volume of PC 1 could be responsible for the excitation of these additional acoustic modes.

- PC 1 showed the highest KI followed by PC 2 and 3, at constant ignition system. The ISP ignition system showed a higher KI compared to the NRP, at constant PC geometry.
- Conventional end gas auto-ignition might not be responsible for knocking events, based on experimental and chemical kinetic simulations data. Specifically, experimental data such as RHR, as well as pressure and temperature at CA of knock onset did not correlate with the trend of KI. Moreover, the range of CA in which end gas auto-ignition was possible, according to chemical kinetics simulations, did not overlap with the CA of knock onset.
- Jets investigated in this work were absolutely unstable; thus, the shear layer between the jets and the surrounding could generate heat release and pressure oscillations. Moreover, a relationship between the normalized entrained mass by the radial PC jets, that relates to the cross-section area of the jets, and the KI has been established for PC 1 and 2. These results highlighted that quenching of the jet-flame impinging on the MC walls could generate heat release and pressure oscillations that could drive knocking events. PC 3 did not satisfy this relationship highlighting that a different nozzle pattern and diameters could have a substantial impact on the jet-flame entrainment.

This work showed that, while PC-based ignition systems can effectively suppress conventional end gas auto-ignition events, pressure fluctuations and knocking events could be generated by jet-related phenomena. Therefore, it is extremely important to further analyze these phenomena to reduce the generated pressure fluctuations and prevent knocking events.

ACKNOWLEDGEMENTS

The authors would like to thank Alberto Garcia for his dedicated support of the Gasoline Combustion Fundamentals Laboratory. Part of this work was performed at the Combustion Research Facility, Sandia National Laboratories, Livermore, CA. Financial support was provided by the U.S. Department of Energy, Vehicle Technologies Office. Sandia National Laboratories is a multi-mission laboratory managed and operated by National Technology and Engineering Solutions of Sandia, LLC., a wholly-owned subsidiary of Honeywell International, Inc., for the U.S. Department of Energy's National Nuclear Security Administration under contract DE-NA0003525. Pablo J. Martinez-Hernandiz was partially supported by an FPI contract (FPI-S2-19-21993) of the "Programa de Apoyo para la Investigación y Desarrollo (PAID-05-19)" of the Universitat Politècnica de València

REFERENCES

[1] G. J. Germane, C. G. Wood, and C. C. Hess, "Lean combustion in spark-ignited internal combustion engines-a review," 1983.

[2] F. A. Ayala, M. D. Gerty, and J. B. Heywood, "Effects of combustion phasing, relative air-fuel ratio, compression ratio, and load on SI engine efficiency," *SAE Trans.*, pp. 177–195, 2006.

[3] L. A. Graham, S. L. Belisle, and P. Rieger, "Nitrous oxide emissions from light duty vehicles," *Atmos. Environ.*, vol. 43, no. 12, pp. 2031–2044, 2009.

[4] N. Hayashi, A. Sugiura, Y. Abe, and K. Suzuki, "Development of ignition technology for dilute combustion engines," *SAE Int. J. Engines*, vol. 10, no. 3, pp. 984–994, 2017.

[5] Y. Ikeda, A. Nishiyama, Y. Wachi, and M. Kaneko, "Research and development of microwave plasma combustion engine (Part I: Concept of plasma combustion and plasma generation technique)," SAE Technical Paper, 2009.

[6] A. Cimarello, C. N. Grimaldi, F. Mariani, M. Battistoni, and M. Dal Re, "Analysis of RF corona ignition in lean operating conditions using an optical access engine," SAE Technical Paper, 2017.

[7] S. Biswas, I. Ekoto, D. Singleton, K. Mixell, and P. Ford, "Assessment of Spark, Corona, and Plasma Ignition Systems for Gasoline Combustion," in *Internal Combustion Engine Division Fall Technical Conference*, 2020, vol. 84034, p. V001T03A015.

[8] W. P. Attard, M. Bassett, P. Parsons, and H. Blaxill, "A new combustion system achieving high drive cycle fuel economy improvements in a modern vehicle powertrain," SAE Technical Paper, 2011.

[9] Q. Malé, G. Staffelbach, O. Vermorel, A. Misdariis, F. Ravet, and T. Poinsot, "Large eddy simulation of pre-chamber ignition in an internal combustion engine," *Flow Turbul. Combust.*, vol. 103, no. 2, pp. 465–483, 2019.

[10] P. Hlaing, M. Echeverri Marquez, V. Shankar, E. Cenker, M. Ben Houidi, and B. Johansson, "A study of lean burn pre-chamber concept in a heavy duty engine," 2019.

[11] R. Novella *et al.*, "Experimental and numerical analysis of passive pre-chamber ignition with EGR and air dilution for future generation passenger car engines," SAE Technical Paper, 2020.

[12] L. Zhou, Y. Song, J. Hua, F. Liu, Z. Liu, and H. Wei, "Effects of different hole structures of pre-chamber with turbulent jet ignition on the flame propagation and lean combustion performance of a single-cylinder engine," *Fuel*, vol. 308, p. 121902, 2022.

[13] W. P. Attard, H. Blaxill, E. K. Anderson, and P. Litke, "Knock limit extension with a gasoline fueled pre-chamber jet igniter in a modern vehicle powertrain," *SAE Int. J. Engines*, vol. 5, no. 3, pp. 1201–1215, 2012.

[14] H. Cui, Z. Zhao, F. Zhang, C. Yu, and L. Wang, "Effect of pre-chamber volume on combustion characteristics of an SI aircraft piston engine fueled with RP3," *Fuel*, vol. 286, p. 119238, 2021.

[15] F. Liu, L. Zhou, J. Hua, C. Liu, and H. Wei, "Effects of pre-chamber jet ignition on knock and combustion

characteristics in a spark ignition engine fueled with kerosene," *Fuel*, vol. 293, p. 120278, 2021.
[16] S. Biswas and L. Qiao, "Prechamber hot jet ignition of ultra-lean H_2/air mixtures: Effect of supersonic jets and combustion instability," *SAE Int. J. Engines*, vol. 9, no. 3, pp. 1584–1592, 2016.
[17] S. Biswas and L. Qiao, "Combustion Instabilities of Ultra-Lean Premixed H 2/Air Mixtures by Prechamber Turbulent Jet Ignition," *J. Propuls. Power*, vol. 34, no. 5, pp. 1166–1177, 2018.
[18] S. Biswas and I. Ekoto, "Detailed investigation into the effect of ozone addition on spark assisted compression ignition engine performance and emissions characteristics," SAE Technical Paper, 2019.
[19] T. Kathrotia, U. Riedel, A. Seipel, K. Moshammer, and A. Brockhinke, "Experimental and numerical study of chemiluminescent species in low-pressure flames," *Appl. Phys. B*, vol. 107, no. 3, pp. 571–584, 2012.
[20] J. Chang, Z. Filipi, D. N. Assanis, and T. Kuo, "New Heat Transfer Correlation for an HCCI Engine Derived from Measurements of Instantaneous Surface...," 2004.
[21] A. J. Shahlari and J. B. Ghandhi, "A comparison of engine knock metrics," SAE Technical Paper, 2012.
[22] A. J. Shahlari and J. Ghandhi, "Pressure-based knock measurement issues," SAE Technical Paper, 2017.
[23] C. S. Draper, *The Physical Effects of Detonation in a Closed Cylindrical Chamber*. Massachusetts Institute of Technology, 1934.
[24] "ANSYS CHEMKIN 17.0 (15151), ANSYS Reaction Design: San Diego, 2016."
[25] S. Cheng *et al.*, "Autoignition and preliminary heat release of gasoline surrogates and their blends with ethanol at engine-relevant conditions: Experiments and comprehensive kinetic modeling," *Combust. Flame*, vol. 228, pp. 57–77, 2021.
[26] J. M. Garcia-Oliver *et al.*, "An experimental and one-dimensional modeling analysis of turbulent gas ejection in pre-chamber engines," *Fuel*, vol. 299, p. 120861, 2021.
[27] F. Di Sabatino, P. J. Martinez-Hernandiz, R. Novella, and I. Ekoto, "Investigation of the Effects of Passive Pre-chamber Nozzle Pattern and Ignition System on the Engine Performance and Emissions," *IJER*, Submitted.
[28] P. J. Martinez-Hernandiz, F. Di Sabatino, R. Novella, and I. Ekoto, "A Numerical and Experimental Investigation on Different Strategies to Evaluate Heat Release Rate and Performance of a Passive Pre-Chamber Ignition System," SAE Technical Paper, 2022.
[29] P. A. Monkewitz, D. W. Bechert, B. Barsikow, and B. Lehmann, "Self-excited oscillations and mixing in a heated round jet," *J. Fluid Mech.*, vol. 213, pp. 611–639, 1990.
[30] A. P. Dowling and Y. Mahmoudi, "Combustion noise," *Proc. Combust. Inst.*, vol. 35, no. 1, pp. 65–100, 2015.
[31] F. P. Ricou and D. B. Spalding, "Measurements of entrainment by axisymmetrical turbulent jets," *J. Fluid Mech.*, vol. 11, no. 1, pp. 21–32, 1961.